

Enhancing Fatigue Detection through Heterogeneous Multi-Source Data Integration and Cross-Domain Modality Imputation

Luobin Cui, Yanlai Wu, Tang Ying, *Senior, IEEE*, and Weikai Li

Abstract—Fatigue detection for human operators plays a critical role in safety critical applications such as aviation, mining, and long haul transport. While numerous studies have demonstrated the effectiveness of high-fidelity sensors in controlled laboratory environments, their performance often degrades when ported to real-world settings due to noise, lighting condition, and field of view constraints, thereby limiting their practicality. This paper formalizes a deployment-oriented setting for real-world fatigue detection, where high-quality sensors are often unavailable in practical applications. To address this challenge, we propose leveraging knowledge from heterogeneous source domains, including high-fidelity sensors that are difficult to deploy in the field but commonly used in controlled environments, to assist fatigue detection in the real-world target domain. Building on this idea, we design a heterogeneous and multi-source fatigue-detection framework that adaptively utilizes the available modalities in the target domain while exploiting diverse configurations in the source domains through cross-domain alignment and modality imputation. Our experiments, conducted using a field-deployed sensor setup and two publicly available human fatigue datasets, demonstrate the practicality, robustness, and improved generalization of our approach across subjects and domains. The proposed method achieves consistent gains over strong baselines in sensor constrained scenarios.

Note to Practitioners—The proposed work is motivated by the growing need for practical and reliable fatigue detection in industrial applications where operator fatigue poses serious safety and productivity risks. While high-performing physiological sensors like EEG provide high-fidelity signals, their use in these environments is limited by constraints such as cost, setup complexity, and sensitivity to environmental conditions. Thus, industry deployment often relies on context-appropriate sensors that may not fully capture fatigue related states. To resolve this gap, we propose a multi-source heterogeneous fatigue detection framework that enables field-deployed systems to take advantage of high-fidelity data collected from controlled environments, even if those modalities are unavailable at deployment. This is achieved through cross-domain alignment and modality imputation. Our experiments validate the practicality, robustness, and generalization of the proposed approach, showing consistent improvements in subject-independent and cross-domain settings.

Index Terms—Fatigue Detection, Sensor Imputation, Data Synthesis

L. Cui and Y. Wu are with the Department of Electrical and Computer Engineering, Rowan University, Glassboro, NJ, 08028 USA (e-mail: cui_luo77@students.rowan.edu, wuyanl37@rowan.edu).

Ying Tang (the corresponding author) is with the Department of Electrical and Computer Engineering, Rowan University, Glassboro, NJ, 08028 USA (e-mail: tang@rowan.edu).

Weikai Li is with the School of Mathematics and Statistics, Chongqing Jiaotong University, Chongqing, 400074 China (e-mail: leeweikai@outlook.com).

I. INTRODUCTION

Physiological responses and behavioral patterns of individuals under fatigue provide rich information to understand the impacts of jeopardized human capacity, from which proper mitigation control can be determined. However, the complexity and vulnerability of data acquisition present several limitations. While the latest advancements of sensor technology have elevated the research of objective fatigue detection to unprecedented levels, concerns about sensor reliability and accessibility remain [1].

Unreliable sensors can result in loss of data, compromising detection accuracy, or, in the worst case, complete malfunction. To address this issue, recent efforts have explored using synthetic data generation strategies to augment incomplete or noisy datasets. For instance, generative AI [2] has emerged as a promising solution. Bird et al. (2021) demonstrated the capability of GPT-2 in generating synthetic electroencephalography (EEG) and electromyography (EMG), which, when combined with real training data, improved classification accuracy [3]. Similarly, research in [4] employed generative adversarial networks (GANs) to enhance data for motor imagery classification in brain-computer interface systems. Along this direct, [5] proposed Generative-DANN (GDANN), a hybrid model that integrates GANs with a Domain-Adversarial Neural Network (DANN) architecture to address cross-subject EEG variability in fatigue detection. By aligning feature distributions across subjects, GDANN improved generalizability and achieved high accuracy in cross-subject fatigue classification tasks. When generating synthetic data for fatigue detection, the process must consider inherent correlations of physiological modalities to collaboratively determine fatigue. To that end, RAINDROP [6] provided a promising approach by using graph neural networks to model these correlations in irregularly sampled and multivariate time-series data.

Although the aforementioned approaches address the challenge of sensor unreliability through data augmentation, few efforts have tackled the equally critical issue of sensor accessibility. In many real-world scenarios, high-end sensors, such as EEG, imaging systems, and pupil dilation monitors, while reliable and accurate, remain prohibitively expensive. The extensive calibration, routine maintenance, and specialized operator training required make these sensors difficult to operate for wide, real-world deployment. Moreover, these sensors are highly sensitive to environmental factors, like noise, lighting condition, and field of view constraints. These sensitivities

complicate data collection and analysis in real-world scenarios, ultimately degrading model accuracy and robustness [7]. As a result, studies involving these sensors are often confined to simulated and controlled environments. For example, high resolution EEG was deployed in a simulated environment, together with heart rate and eye blink rate, to analyze mental fatigue or drowsiness during car driving [8]. However, such simulation based setups often fail to capture the complexity and uncertainty of actual driving conditions [9], which in turn limits the generalizability of models trained in these idealized environments. Nonetheless, transferring knowledge gained from controlled settings remains valuable, provided it is adapted appropriately, offering a foundation for practical fatigue detection in real-world scenarios where direct sensor deployment is constrained. Note that this type of transfer requires a form of cross-domain adaptation that goes beyond the capabilities of existing generative methods. Current approaches, such as GANs and GPT-based models mentioned earlier, have proven effective for within-domain synthesis, where additional data is generated for modalities already present at both training and deployment (e.g., generating more EEG from partial EEG). However, they are not designed for cross-domain transfer with target-never-seen modalities, where an entire sensor modality is absent in the target domain at both training and deployment, for example, leveraging EEG-related knowledge when no EEG has ever been observed in the target system. This limitation highlights a critical gap: the need for methods that can support cross-domain sensor transfer to address real-world sensor accessibility constraints.

Motivated by these remarks, this paper proposes a novel domain-adaptive framework that enables real-world fatigue detection systems to learn from and be enhanced by controlled-environment data, even when the data originate from entirely different sensor sources. This approach offers a practical solution by facilitating cross-domain knowledge transfer, extending the utility of high-fidelity but deployment-constrained sensors to settings where they are otherwise unavailable. To this end, we present the framework with the following core contributions:

- A practical yet underexplored problem setting for real-world fatigue detection is formally defined. This definition reflects the need to operate fatigue detection systems with context-appropriate, accessible sensors in the field while leveraging knowledge transferred from differently instrumented, high-fidelity but deployment-constrained sensor sources (e.g., EEG or ECG collected in controlled lab environments). It captures the central challenges of modality heterogeneity, incompleteness, and domain shift, and lays the foundation for developing models that can generalize across mismatched sensor configurations in diverse deployment contexts.
- A heterogeneous and multi-source fatigue detection framework is proposed and validated as a solution to this problem. Grounded in a thorough theoretical analysis, we explore the conditions under which knowledge from differently instrumented source domains can be effectively leveraged to support fatigue prediction in a target

domain. A domain-adaptive model is then developed to dynamically integrate available target-domain modalities while leveraging complementary information from multiple source domains. The design enables accurate fatigue prediction in real-world settings even under constrained sensor configurations. The framework and the model are validated using a practical sensor configuration and two publicly available datasets, demonstrating improved generalization and overall performance.

II. RELATED WORK

This section reviews key developments in fatigue assessment. Section II.A examines existing fatigue detection methods, highlighting their advantages and limitations, which underscore the need for a new approach that builds on strengths while addressing shortcomings. Section II.B explores the current data generation methods in mitigating data scarcity, along with their constraints in practical applications. Finally, Section II.C discusses the use of open datasets for fatigue assessment and the associated challenges with sensor discrepancies and label heterogeneity.

A. Fatigue Assessment

Traditional fatigue assessment methods are based on subjective evaluation tools, including self-reports and questionnaires. Since the last century, numerous classic fatigue assessment scales have been widely utilized, including the Stanford Sleepiness Scale (SSS) [10], proposed by Stanford University; the Multidimensional Fatigue Inventory (MFI) [11], developed by Smets et al.; and the International Fitness Scale (IFIS) [12], which measures changes in overall vigor and affect. These scales encompass a multitude of dimensions of fatigue and serve as the foundation for traditional fatigue assessment. Nevertheless, both questionnaires and self-reports are highly influenced by an individual's psychological state and external environment, resulting in subjective and inconsistent outcomes [13]. Moreover, most of these methods [14]–[16] are post hoc assessments, making them unsuitable for real-time fatigue monitoring and preventive measures—both of which are essential in high-stakes environments, such as driving [17] and aviation [18].

To address these limitations, researchers have explored more objective measures of human fatigue. In fact, a person's fatigue state can be reflected in changes in physiological signals, such as heart rate (HR), heart rate variability (HRV), electrocardiogram (ECG), EEG [19] [20], galvanic skin response (GSR), skin temperature (ST), blood pressure (BP), EMG [21], [22] and blood oxygen saturation (SpO₂). Studies have shown that when drivers enter a fatigued state, their HRV metrics change significantly. Notably, a decrease is often observed in the time domain on measures such as how much the time between heartbeats naturally varies and how much consecutive heartbeats differ from each other. This suggests that the ability of the body to regulate heart activity is weakened. Similarly, HRV indicators in the frequency domain, such as the low-frequency and high-frequency ratios, often become unstable, reflecting an imbalance in the regulatory function

of the autonomic nervous system [23]. Additionally, GSR signals during fatigue are usually characterized by a rise in baseline conductance level and response fluctuations, which is closely correlated to enhanced sympathetic nerve activities [24]. Through real-time monitoring and joint analysis of these specific indicators, the subtle changes in the driver's physiological state can be captured more precisely, thus significantly improving the sensitivity and accuracy of the fatigue detection system [25]. With technological advancement, physiological signal acquisition devices are becoming smaller and more user-friendly, significantly driving research in real-time fatigue monitoring [26].

Among various physiological signals, EEG has gained popularity in fatigue detection due to its ability to directly measure brain activity with high accuracy. However, traditional EEG systems are expensive, require an intrusive setup and specialized personnel for operation, making it challenging for real-world deployment. As a result, the majority of EEG-based fatigue studies remain confined to controlled laboratory settings [27]–[29]. Although portable EEG devices have emerged for field applications, their data quality is not as good as that of laboratory-grade devices. Additionally, they are susceptible to external noise and interference, significantly impacting their stability and detection accuracy [30], [31].

In response to these challenges, researchers have explored noninvasive alternatives, leading to the increase of vision-based fatigue detection [32]. These methods assess fatigue by analyzing facial features, such as eyelid closure time [33], yawning frequency [34], and body movement [35], [36] from images captured by cameras in real time. Despite their many advantages, these methods also face challenges, such as lighting variations and camera angles, which can affect image quality and ultimately detection accuracy. In addition, long-term monitoring human subjects' facial and body movements in work environments raises privacy concerns [37] and may lead to employee resistance. Along with this trend, alternative visual signals, like pupil dilation and gaze tracking, have gained attention in the field of fatigue detection. Eyes are often considered as the most intuitive window of the mental state, which can directly reflect the immediate response to fatigue and show high accuracy in fatigue assessment. Studies have shown that pupil diameter and gaze focus are important indicators for assessing workload and fatigue status [38]–[40], including our own study [41] to collect human eye and physiological data for combined fatigue detection. However, while pupil dilation and gaze tracking offer promising insights, they are also sensitive to external environmental factors. Pupil dilation can be influenced by ambient lighting conditions, which may reduce its reliability in dynamic or uncontrolled environments. Similarly, gaze tracking can be affected by head movements, occlusions, and variations in camera positioning, limiting its stability and accuracy unless the camera is confined to a controlled environment, such as the one in our study [41] using HoloLens.

In summary, different sensor signals possess distinct advantages in fatigue detection, with some proving more effective than others. However, their effectiveness is highly contingent on applications and settings. For example, EEG performs well

in controlled settings but can be challenging to deploy in real world contexts due to susceptibility to noise and constraints on setup and usability. Although commercial wearable EEG systems exist, practical use outside the lab often requires additional artifact handling and user training. Similar sensitivity issues rule out the use of pupil dilation in practical applications, and require the use of gaze tracking within a confined setup. Therefore, researchers usually select available and/or context-appropriate resources to collect signals that best align with their research objectives. Even so, we should not overlook the value of the knowledge learned from settings where these context-inappropriate sensors have been effectively applied. If a mechanism exists to transfer that knowledge, it could be used to augment fatigue detection in environments where those sensors are unavailable or impractical, thereby preserving their contribution without requiring their direct deployment.

B. Data Synthesis Methods

Data synthesis, a technology that generates artificial data that maintains the statistical or structural characteristics of real datasets, has demonstrated significant advantages in dealing with data scarcity in recent years. This is particularly relevant in physiological signal analysis, where data collection can be challenging due to various factors such as sensor availability, sensitivity to noise, and subject-related variability, leading to widespread adoption in this domain [42].

Early developments in data synthesis (DS) primarily leveraged statistical regression techniques, where synthetic data was generated through parameterized modeling of observed data distributions. For instance, Linear regression and Bayesian regression were among the first approaches adopted to model temporal dependencies and fill in missing physiological signals by assuming probabilistic relationships among features [43]. As datasets grew in complexity and dimensionality, regularized models such as ridge regression [44] and lasso regression [45] were introduced to improve generalization. However, despite these advancements, statistical models remained fundamentally limited in their ability to capture long term dependencies and nonlinear temporal dynamics, which are prevalent in complex physiological signals.

Deep learning, on the other hand, has provided promising solutions to this challenge. Recurrent Neural Networks (RNNs), particularly Long Short-Term Memory (LSTM) networks, have proven effective in capturing long-term temporal dependencies in multivariate time-series data. Several studies have demonstrated their success in a variety of applications, such as GRU-D, which incorporates decay mechanisms and masking for clinical time-series data [46]; an LSTM-based imputation model for ECG signals that outperforms classical methods [47]; and BRITS, which enables bidirectional gradient-based imputation without strong distributional assumptions [48]. In parallel, Convolutional Neural Networks (CNN) have shown great success in extracting local spatial and temporal features. Their strength has inspired hybrid models that combine CNNs with LSTMs to jointly leverage spatial and temporal dependencies for more accurate imputation and signal reconstruction [49]. Additionally, GANs have emerged

as a leading approach for producing high-fidelity synthetic signals that are statistically indistinguishable from real ones. Examples can be found in [50], [51] [52].

Despite this progress, current DS techniques across both classical and deep learning paradigms typically operate under a critical limitation: they rely solely on observed data from a single modality or domain to infer or generate new data of the same type. This assumption restricts their generalizability and limits their ability to model cross domain relationships or synthesize data from unseen modalities or sources, which is especially problematic in real world physiological settings, where data is not only sparse and incomplete, but also highly heterogeneous across domains, such as different sensing devices, sensing modalities, and subject populations. Overcoming this constrain is essence of our work, which aims to enable more flexible and adaptive synthesis by integrating knowledge across both domains and modalities.

C. Open Fatigue Detection Datasets

A review of relevant literature has identified several open datasets for fatigue detection. As shown in Table I, the use of diverse physiological signals reaffirms that researchers tend to select sensors that are readily accessible and convenient. Meanwhile, certain signals recur across datasets, including HR, PPG, EDA, acceleration (ACC), and ST.

The commonality and diversity across datasets present both challenges and opportunities. For example, while FatigueSet [53], MEFAR [54], and VPFD [41] share similar data types, they use different sensors—Empatica E4 for the first two datasets and Google Pixel Watch 2 for the third. These variations in data collection methods, sensor specifications, and pre-processing can hinder standardization and generalization.

In addition to these sensor-level discrepancies, label heterogeneity also presents a major challenge for joint modeling and cross-dataset transfer. For instance, some datasets use continuous fatigue scores, whereas others rely on binary labels such as “fatigued” or “not fatigued.” Even among continuous labels, threshold definitions may differ (e.g., fatigue defined as scores > 3 or > 5 on a subjective scale). These inconsistencies need to be addressed to enable more consistent model transfer across datasets.

FatigueSet [53] and MEFAR [54], collected under controlled laboratory conditions, include high-fidelity signals—such as EEG in both datasets and ECG in FatigueSet—that are often impractical for real-world deployment. In contrast, the VPFD [41] dataset was designed for real-world use and thus relies on more accessible sensors except for EEG and ECG. This distinction directly motivates our evaluation of the central hypothesis posed in the Introduction: Can fatigue-relevant knowledge learned from high-resolution EEG and ECG sources be effectively transferred to enhance fatigue prediction in settings like VPFD, where only context-appropriate sensors are available? Note that the three datasets provide a relatively homogeneous foundation for our evaluation, as all rely on self-reported binary fatigue scores. The only distinction lies in FatigueSet, which separates mental and physical fatigue, whereas MEFAR and VPFD do not. For consistency across

datasets, we combined both mental and physical fatigue into a unified label. In the following sections, we present the results of this exploration.

III. HETEROGENEOUS AND MULTI SOURCE FATIGUE DETECTION FRAMEWORK

A. Problem Definition

We consider a fatigue detection task in the presence of heterogeneous, incomplete, and multi-source sensor data. Specifically, assume there exists:

- A target domain dataset $\mathcal{D}_T = \{(x_T^{(i)}, y_T^{(i)})\}_{i=1}^{n_T}$ with limited samples, where $x_T^{(i)} \in \mathbb{R}^{d_T}$ represents the sensor feature vector defined over \mathcal{X}_T and $y_T^{(i)} \in \mathcal{Y}$ is the label. n_T is the number of target samples and d_T is the number of feature dimensions, i.e., number of sensors.
- A collection of source domains $\{\mathcal{D}_s\}_{s=1}^S$, where each $\mathcal{D}_s = \{(x_s^{(i)}, y_s^{(i)})\}_{i=1}^{n_s}$ contains samples from a different sensor configuration or environment. Each $x_s^{(i)} \in \mathbb{R}^{d_s}$ is defined over \mathcal{X}_s and $y_s^{(i)} \in \mathcal{Y}$. S is the number of source domains, n_s is the number of samples in source domain s , and d_s is the feature dimensionality of \mathcal{D}_s .

In the context of our problem, heterogeneous refers to the differences in the feature spaces and data distributions across different domains. Specifically, the feature spaces (i.e., the set of sensors or features) and the data distributions (i.e., the statistical properties of the data) in the target domain and source domains are not identical. This can be formally defined as follows:

- Feature Space Heterogeneity: For each source s , $\mathcal{X}_T \neq \mathcal{X}_s$ may hold while $\mathcal{X}_T \cap \mathcal{X}_s \neq \emptyset$; when $\mathcal{X}_T = \mathcal{X}_s$, our setting reduces to an identical-modality special case (no imputation required).
- Data Distribution Heterogeneity: $\mathbb{P}_T \neq \mathbb{P}_s$ for $s = 1, \dots, S$, where \mathbb{P}_T and \mathbb{P}_s denote the distributions of target and source domains, respectively.

Since the obtained sensors tend to be heterogeneous across different domains in the data collection process. Thus, we have

- $\mathcal{X}^\cap := \mathcal{X}_T \cap \mathcal{X}_s$
(common sensors between \mathcal{D}_T and \mathcal{D}_s)
- $\mathcal{X}^{s-} := \mathcal{X}_T \setminus \mathcal{X}^\cap$
(sensors present in \mathcal{D}_T but missing in \mathcal{D}_s)
- $\mathcal{X}^{s+} := \mathcal{X}_s \setminus \mathcal{X}^\cap$
(sensors present in dataset \mathcal{D}_s but missing in \mathcal{D}_T)

Here, we assume that each sensor, regardless of its type or modality, is available in at least one domain. Besides, we also have $\mathbb{P}_T^\cap \neq \mathbb{P}_s^\cap$, where \mathbb{P}_T^\cap and \mathbb{P}_s^\cap is the distribution over \mathcal{X}^\cap of \mathcal{D}_T and \mathcal{D}_s , respectively. Here, our task is to enhance the performance of a fatigue detector f in the target domain by leveraging data from multiple heterogeneous source domains. Specifically, under distribution shift, we seek to generate the features missing in the target domain by leveraging multiple heterogeneous source datasets, thereby enhancing the model’s fatigue-detection performance. For completeness, for each source s we learn a modality-imputation mapping $g_s : \mathcal{X}^\cap \rightarrow \mathcal{X}^{s+}$ on \mathcal{D}_s , construct $\hat{a}_T^{(s)} := g_s(x^\cap)$, and form

TABLE I: Summary of fatigue detection datasets and acquisition devices

Dataset	Human Subjects	Hours	Data Types											
			PPG	GSR	HR	ST	ACC	EYE	EEG	ECG	EMG	BP	FACE	
CogBeacon [55]	19	35							✓					✓
CLAS [56]	62	31	✓	✓	✓						✓			
MePhy [57]	60	8		✓					✓		✓	✓		✓
OperEYEV [58]	10	10			✓				✓				✓	✓
WESAD [59]	15	13	✓	✓	✓	✓	✓	✓			✓	✓		
FatigueSet [53]	12	13	✓	✓	✓	✓	✓	✓		✓	✓			
MEFAR [54]	23	28	✓	✓	✓	✓	✓	✓		✓				
VPPFD [41]	4	9	✓	✓	✓	✓	✓	✓	✓					

the augmented target feature $\hat{x}_T^{(s)} = [x^\cap, \hat{a}_T^{(s)}]$. In the multi-source case, we concatenate or fuse the reconstructed features $\{\hat{a}_T^{(s)}\}_{s=1}^S$ to obtain the final augmented representation.

B. Theoretical Analysis

To gain a deeper understanding of the problem and our proposed solution, we theoretically analyze the generalization bound associated with it. For simplicity and ease of understanding, in our theoretical analysis, we only considered one source domain, which can readily extend to multiple source domains without additional conceptual difficulty. For a random variable x generated from a distribution \mathbb{P} , we use $\mathbb{E}_{x \sim \mathbb{P}}$ to denote the expectation taken over x with distribution \mathbb{P} . The expected generalization error of the Fatigue Detector $f(x)$ is $\mathcal{E}_{\mathbb{P}}(f)$, while the empirical generalization error is the $\mathcal{E}_{\hat{\mathbb{P}}}(f)$. Throughout this section, $I(x; y)$ denotes mutual information between the labels y and the training features x , i.e., sensors in our task.

Lemma III.1. [60] *Suppose the loss function $\mathcal{L}(f(x), y)$ is R -sub-Gaussian under $x \sim \mathbb{P}$ for all $y \in \mathcal{Y}$, then, we have:*

$$\mathcal{E}_{\mathbb{P}}(f) \leq \mathcal{E}_{\hat{\mathbb{P}}}(f) + \sqrt{\frac{2R^2}{n}} I(x; y) \quad (1)$$

Let a denote a label-related advanced sensor and \hat{a} its imputed counterpart. Define $x^+ = [x, a]$ with joint distribution \mathbb{P}_+ over (x^+, y) , and $\hat{x}^+ = [x, \hat{a}]$ with joint distribution \mathbb{Q} over (\hat{x}^+, y) .

Theorem 1. *Assume that x, a are independent of each other, $x \sim \mathbb{P}, a \sim \mathbb{Q}_a$, while both being conditionally dependent on variable of y . Let the composite observation be defined as $x^+ = [x, a], x^+ \sim \mathbb{P}_+$, with the incorporating the variable a , the $\mathcal{E}_{\mathbb{P}_+}$ have a tighten upper bound than $\mathcal{E}_{\mathbb{P}}$, the gap G is:*

$$G = \Delta + \sqrt{\frac{2R^2}{n}} \left(\sqrt{I(x^+; y)} - \sqrt{I(x; y)} \right) < 0 \quad (2)$$

where $\Delta = \mathcal{E}_{\hat{\mathbb{P}}_+} - \mathcal{E}_{\hat{\mathbb{P}}}$. The proof is given in the appendix. Following Theorem 1, it is evident that incorporating label-related features/sensors (i.e., a) can effectively reduce the generalization error bound, thereby enhancing the generalization performance. This result validates the critical necessity of incorporating/generating advanced sensors into our fatigue detection task.

Theorem 2. *Given a random variable \hat{a} generated from a distribution $\mathbb{Q}_{\hat{a}}$, and $\hat{x}^+ = [x, \hat{a}] \sim \mathbb{Q}$, then we have:*

$$\mathcal{E}_{\mathbb{P}_+}(f) \leq \mathcal{E}_{\hat{\mathbb{Q}}}(f) + \epsilon_{ideal} + d_{\mathcal{H}\Delta\mathcal{H}}(\mathbb{Q}_a, \mathbb{Q}_{\hat{a}}) + \sqrt{\frac{2R^2}{n}} I(x; y) \quad (3)$$

where $\mathcal{E}_{\hat{\mathbb{Q}}}(f)$ is the empirical generalization error over distribution \mathbb{Q} , $d_{\mathcal{H}\Delta\mathcal{H}}(\mathbb{Q}_a, \mathbb{Q}_{\hat{a}})$ is the $\mathcal{H}\Delta\mathcal{H}$ distance between \mathbb{Q}_a and $\mathbb{Q}_{\hat{a}}$. \mathbb{P}_+ represent the distribution over the feature x^+ . The proof is given in the Appendix.

Through Theorem 1 and Theorem 2, it is evident that without additional sensors a , if the distribution distance between \mathbb{Q}_a and $\mathbb{Q}_{\hat{a}}$, is less than a constant, i.e., $d_{\mathcal{H}\Delta\mathcal{H}}(\mathbb{Q}_a, \mathbb{Q}_{\hat{a}}) \leq \left| \sqrt{\frac{2R^2}{n}} \left(\sqrt{I(x^+; y)} - \sqrt{I(x; y)} \right) - \Delta - \epsilon_{ideal} \right|$, we can obtain a tighter generalization error bound, thereby improving the generalization performance of the model. This result validates that generating advanced sensors can enhance the performance of fatigue detection.

Thus, to effectively enhance model performance, we are motivated to minimize the distributional discrepancy $d_{\mathcal{H}\Delta\mathcal{H}}(\mathbb{Q}_a, \mathbb{Q}_{\hat{a}})$ between generated sensor \hat{a} and potential real sensor a by training a regression model $g_s : \mathcal{X}^\cap \rightarrow \mathcal{X}^{s+}$ over \mathcal{D}_s . Since the $\mathcal{H}\Delta\mathcal{H}$ distance is symmetric, obeys the triangle inequality, and is bounded, we can regard it as a loss function ℓ . Following the current theoretical work, [61]. We easily have the following results.

Theorem 3. *Let \mathcal{H} be a hypothesis class. $R_s^\ell(g)$ and $R_T^\ell(g)$ denote the expected loss of loss function ℓ for the source and target domains. for $g_s^* = \arg \min_{g \in \mathcal{H}} R_s^\ell(g)$ and $g_T^* = \arg \min_{g \in \mathcal{H}} R_T^\ell(g)$ denoting the ideal hypotheses for the source and target domains, we have*

$$R_T^\ell(g_s) \leq R_S^\ell(g_s, g_s^*) + d_{\mathcal{H}\Delta\mathcal{H}}(\mathbb{P}_T^\cap, \mathbb{P}_S^\cap) + \epsilon, \quad (4)$$

where $R_S^\ell(g_s, g_s^*) = \mathbb{E}_{x \sim \mathbb{P}_S} \ell(g_s(x), g_s^*(x))$ and $\epsilon = R_T^\ell(g_T^*) + R_S^\ell(g_T^*, g_s^*)$. Since \hat{a} is generated by g_s . The $d_{\mathcal{H}\Delta\mathcal{H}}(\mathbb{Q}_a, \mathbb{Q}_{\hat{a}})$ is bounded by $R_S^\ell(g_s, g_s^*)$ and $d_{\mathcal{H}\Delta\mathcal{H}}(\mathbb{P}_T^\cap, \mathbb{P}_S^\cap)$. Following this idea, to reduce the distributional discrepancy $d_{\mathcal{H}\Delta\mathcal{H}}(\mathbb{Q}_a, \mathbb{Q}_{\hat{a}})$, we also require to reduce the distribution gap $d_{\mathcal{H}\Delta\mathcal{H}}(\mathbb{P}_T^\cap, \mathbb{P}_S^\cap)$.

C. Learning Objective

Motivated by Theorem 1 and 2, we provide our heterogeneous and multi source framework. Specifically, given a target

domain \mathcal{D}_T , our learning objective is to detect fatigue with knowledge transferring from multiple source domains (e.g., high fidelity knowledge extracted from controlled environments) $\{\mathcal{D}_s\}$ for $s = 1, \dots, S$. Here, as a naive attempt, we aim to transfer knowledge by utilizing the remaining domains to generate the missing sensors (i.e., \mathcal{X}^{s+}) in \mathcal{D}_s . The learning objective is defined as follows:

$$\mathcal{L} = \min_{g_s, f} \sum_{s=1}^S \underbrace{\mathbb{E}_{\mathcal{D}_s} [\mathcal{L}_{rec}(g_s(\mathcal{X}^\cap, \mathcal{X}^{s+}))]}_{\text{Sensor Reconstruction}} + \underbrace{[\mathcal{L}_{dis}(\mathbb{P}_T^\cap, \mathbb{P}_s^\cap)]}_{\text{Domain Alignment}} \quad (5)$$

$$+ \underbrace{\mathbb{E}_{\mathcal{D}_T} [\mathcal{L}_{task}(f(\tilde{\mathcal{X}}_T), y)]}_{\text{Task Aware Detection}}$$

where g_s is the feature generator for generating \mathcal{X}^{s+} , f is the classifier function for fatigue detection. \mathcal{L}_{rec} represents the reconstruction loss (e.g., MSE for regression). \mathcal{L}_{task} denotes the task specific loss (e.g., MSE for regression, CE for classification), $\tilde{\mathcal{X}}_T$ represents the reconstructed data from domain \mathcal{D}_T . This data has been enhanced or completed using the information generated by the feature generator g_s from other domains.

Moreover, motivated by Theorem 3, we introduce a domain alignment term to reduce $d_{\mathcal{H}\Delta\mathcal{H}}(\mathbb{P}_T^\cap, \mathbb{P}_s^\cap)$. Specifically, a batch normalization step [62], referred to as *BatchNorm*, is applied before fusion. Additionally, to optimize the objective function in Equation 5, particularly the task specific loss, we adopt the Jacobian Norm Regularization method [63] referred to as *JacobianNorm* later.

D. Framework

For the problem defined above, we propose a framework that enables cross-domain knowledge integration to improve fatigue detection under heterogeneous sensor configurations. The overall framework is given in Fig.1, with the detailed procedures outlined in Algorithm 1. The method is designed to handle data collected from different sensor configurations with partially overlapping feature spaces. When new data from a different sensor setup becomes available, the framework compares its feature space to that of the target domain. If discrepancies are found—i.e., missing modalities—the method initiates a targeted imputation process to infer the missing signals. This imputation process is detailed in Algorithm 2 and illustrated in Fig.2. The aligned and augmented data is then incorporated into the model to enhance prediction accuracy in the target domain as illustrated in Fig.3.

Algorithm 1 Multi source Fatigue Detection

Require: Target dataset \mathcal{D}_T , source datasets $\{\mathcal{D}_s\}_{s=1}^S$
Ensure: Detector f trained on enhanced target data

- 1: **for** $s = 1$ **to** S **do**
- 2: Compute shared and unshared features: $\mathcal{X}^{s-}, \mathcal{X}^{s+}$ w.r.t. $(\mathcal{D}_T, \mathcal{D}_s)$
- 3: $\mathcal{D}_T \leftarrow \text{SENSORIMPUTE}(\mathcal{D}_T, \mathcal{D}_s)$
- 4: **end for**
- 5: Train detector f_ϕ on final enhanced \mathcal{D}_T

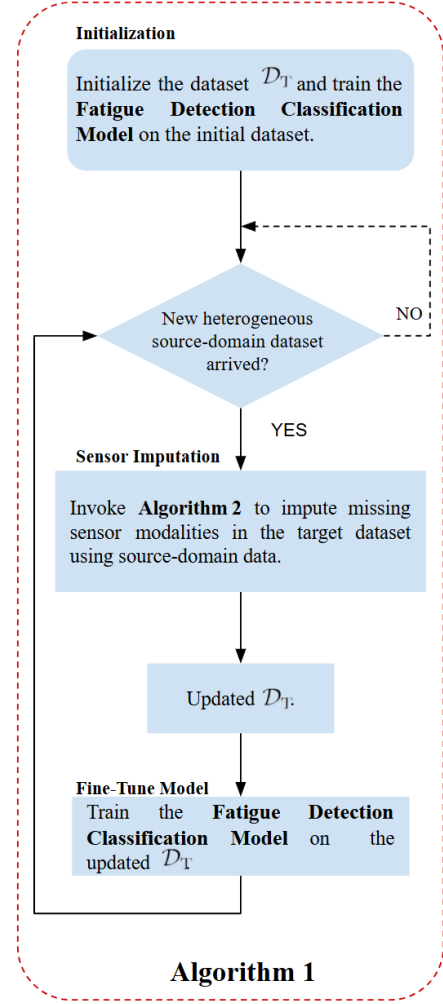


Fig. 1: Overall framework.

Algorithm 2 SENSORIMPUTE($\mathcal{D}_T, \mathcal{D}_s$)

Require: Reference dataset \mathcal{D}_T , auxiliary source dataset \mathcal{D}_s

Ensure: Updated target dataset \mathcal{D}_T

- 1: Compute modality difference sets

$$\mathcal{X}^{s-} = \mathcal{X}_T \setminus \mathcal{X}_s, \quad \mathcal{X}^{s+} = \mathcal{X}_s \setminus \mathcal{X}_T$$

- 2: **if** $\mathcal{X}^{s+} \neq \emptyset$ **then**
 - 3: Apply g_s to impute missing features \mathcal{X}^{s+} in \mathcal{D}_T based on \mathcal{D}_s
 - 4: **end if**
 - 5: return \mathcal{D}_T
-

IV. EXPERIMENTS

A series of experiments are designed to validate our framework. Section IV.A details the experimental setup, including the selected dataset, environment, and data preprocessing. Section IV.B describes the experimental design and discusses the results.

A. Experimental Setup

For the experiments to be elaborated in a later subsection, three datasets containing various physiological signals some

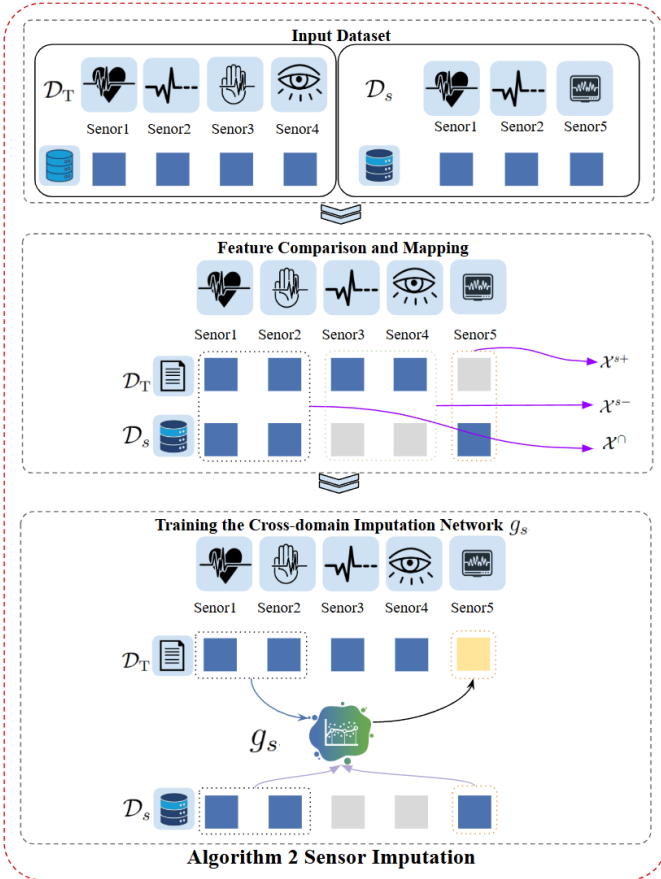


Fig. 2: Sensor Imputation Module.

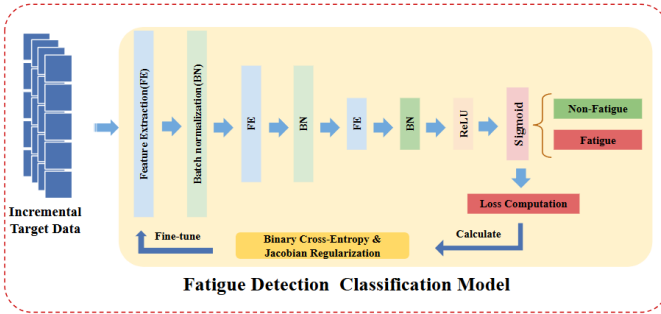


Fig. 3: Fatigue Detection model.

overlapping and others unique are selected. Meanwhile, three widely used classification methods are chosen, utilizing both individual datasets and the enhanced target data for training. To minimize discrepancies and enhance the usability of these datasets, data pre-processing is required before prior to experimentation. To that end, we describe the selected datasets, implementation environment, and the data pre-processing steps in detail.

1) *Datasets*: Out of all publicly available datasets for fatigue, VPFD [41], MEFAR [54] and FatigueSet [64] are chosen for our experiments because they share a large set of overlapping physiological signals while each also contains unique ones. For instance, all of three datasets include HR, PPG, GSR, ST, and ACC. Additionally, MEFAR provides EEG

data, FatigueSet includes both EEG and ECG data, and VPFD offers unique eye-tracking data.

- VPFD dataset [41] is a multimodal fatigue detection dataset designed to reflect practical deployment conditions. It was collected using wearable devices like the HoloLens and Google Pixel Watch 2. The dataset contains physiological signals from four 27 year old participants monitored for up to 9 hours during sports, driving, and research activities.
- MEFAR dataset [54] focuses on occupational mental fatigue analysis. It comprises neurophysiological data from 23 participants across four occupational groups (i.e., academicians, technicians, engineers, and kitchen workers). The EEG signals were captured by the NeuroSky MindWave, while other signals were recorded by the Empatica E4 wristband.
- FatigueSet dataset [64] contains data from 12 participants performing controlled physical and cognitive tasks. It utilizes the Muse S headband for EEG signals, the Zephyr BioHarness chestband for ECG signals, and the Empatica E4 wristband for the rest of physiological signals.

2) *Implementation Environment and Data Preprocessing*:

Experiments are executed on a high performance PC featuring an Intel Core i9-14900K processor, NVIDIA RTX 4090 GPU, and 128GB of RAM. The system operates on Windows 11, with a software stack comprising Python 3.10.15, PyTorch 2.4.1, scikit-learn 1.1.3, pandas 2.2.2, and numpy 1.26.4.

To minimize noise and artifacts, we apply a series of tailored preprocessing techniques to each signal type. Specifically, ACC and PPG signals are processed using Recursive Least Squares (RLS) and Single channel Signal Analysis (SSA) to effectively remove motion artifacts while preserving critical physiological features. HR, GSR, and ST signals undergo Maximum Outlier Filtering to eliminate extreme values and ensure data smoothness. Additionally, all signals are resampled to 32 Hz to standardize sampling rates across various devices.

For all datasets, a participant-specific normalization strategy is implemented. Each subject's data is normalized individually to mitigate inter-subject physiological variability, ensuring that all target-domain samples reside in a unified feature space, thereby enhancing model comparability and training stability.

Before conducting the experiments, we preprocess the dataset and divide it into an 80% training set and a 20% test set using a block-based strategy rather than random splitting. Specifically, the data is first segmented into continuous blocks based on changes in fatigue labels. For instance, if biometric data is collected from 15 participants, each participant's data forms a block. From each block, we select 20% of the data for the test set by taking the first 10% and the last 10%. Combined, these selections constitute 20% of the entire dataset, preserving the temporal order and capturing all states without shuffling.

For all experiments described below, except for the sensitivity test, the learning parameters are initialized as listed in Table II.

B. Experimental Design and Results

1) *Regression Based Imputation Model Selection*: Without loss of generality, the first set of experiments validates our

TABLE II: Hyperparameters for Imputation and Classification

Parameter	Imputation Phase	Classification Phase
Learning rate	1e-3	3e-4
Batch size	512	256
Optimizer	Adam	Adam
Dropout rate	-	0.2
Max epochs	2000	200
Early stopping patience	40	20

imputer selection by assessing its ability to recover a single blocked modality. We compare four regression architectures—MLP, LSTM (Long Short Term Memory), CNN1D, and TimeMixer [65] on two datasets: FatigueSet (with ECG masked) and MEFAR (with EEG masked). In each case, the missing channel is replaced by the model prediction, and we record the mean squared error (MSE). All errors are computed on strictly held-out, non-overlapping 10-s windows sampled at 32 Hz. The results illustrate that the MLP consistently yields the lowest MSE as shown in Table III. Consequently, the MLP serves as the default model for all subsequent modality imputation tasks, unless otherwise specified.

TABLE III: Regression performance of different models

Model	FatigueSet-ECG(MSE)	MEFAR-EEG(MSE)
CNN1D	0.5063	0.1031
MLP	0.4074	0.1028
LSTM	0.4250	0.1076
TimeMixer	0.5508	0.5455

2) *Validity of Regression-Imputed Data Versus Noise Baselines*: The second set of experiments is designed to not only verify Theorems 1 and 2 but also demonstrate that imputed data can effectively support classifier tasks. In this case, VPFD is chosen with its gaze modality masked and reconstructed using three different methods: MLP-predicted values, MLP prediction with Gaussian noise, and pure random noise. We refer to the modified datasets as $VPFD_{MLP}$, $VPFD_{MLP+noise}$, and $VPFD_{noise}$, respectively. The added noise follows a zero-mean Gaussian distribution whose standard deviation is twice the largest absolute value in the original VPFD gaze data. Finally, we train four separate MLP classifiers using 80% of the original VPFD dataset and each of the three modified versions, respectively. All models are evaluated on the same test set—20% of the original VPFD data—to ensure a consistent basis for comparison. Table IV clearly shows that the classifier trained on regression-generated data maintains a similar performance to the one trained on the original data. This demonstrates the potential of data synthesis as a solution for addressing missing data. However, the introduction of noise, whether partial or complete, increases the distribution difference between the original and generated data, leading to degraded classifier performance.

3) *Impact of Cross-Domain Imputed Modalities on Classification Performance*: The third set of experiments evaluates the VPFD dataset across different scenarios, where modalities are reconstructed from two auxiliary sources: FatigueSet and MEFAR using various augmentation methods and evaluated with multiple classifiers.

TABLE IV: Classification performance on different training datasets.

Training Dataset	Cross-Entropy Loss	Accuracy (%)
VPFD	1.2789	81.15
$VPFD_{MLP}$	1.5523	80.00
$VPFD_{MLP+noise}$	1.2041	60.58
$VPFD_{noise}$	1.6507	60.15

We first train the fatigue detector f_ϕ on the unmodified VPFD to obtain the baseline. Next, we run Algorithm 1 under three configurations of auxiliary source availability with the MLP and TimeMixer serving as imputers, respectively: (a) only FatigueSet is available, which is used to impute the missing ECG modality, resulting in the variant referred to as VPFD w/ ECG (MLP) and VPFD w/ ECG (TimeMixer); (b) only MEFAR is available, used to reconstruct the missing EEG channel, producing the variant termed as VPFD w/ EEG (MLP) and VPFD w/ EEG (TimeMixer); and (c) both FatigueSet and MEFAR are available, enabling the sequential reconstruction of ECG and EEG for the VPFD w/ ECG+EEG (MLP) and VPFD w/ ECG+EEG (TimeMixer) variants. In all cases, the original VPFD features are preserved, and only the missing channels are imputed and appended. Again, each dataset is split, with 80% used to train a classifier and the remaining 20% used for evaluation.

To assess the robustness and generalizability of our approach across model architectures, we train four different classifiers in this experiment—MLP, LSTM, CNN1D, and a Transformer—on each dataset variant. We assess performance using multiple metrics, including accuracy, binary F1, Area Under the ROC Curve (ROC AUC), Area Under the Precision-Recall Curve (PR AUC), macro F1, weighted F1, expected calibration error (ECE), and Brier score. This setup allows us to evaluate not only how each additional reconstructed modality—individually or in combination—contributes to downstream fatigue detection performance, but also the effectiveness of our framework across diverse classifier types.

Table V summarizes the classification metrics under these scenarios. The results demonstrate that our targeted imputers effectively recover missing modalities and that each added channel contributes to and enriches feature representations, thereby boosting fatigue detection performance. Importantly, this feature-level augmentation enables leveraging knowledge derived from high-fidelity but deployment-constrained sensors (e.g., ECG and EEG), thereby strengthening the performance of the practical sensor configuration (i.e., VPFD) without modifying its original features. It is interesting to note that when used individually, neither the TimeMixer, a more advanced imputer, nor the Transformer, a more advanced classifier, yields consistent improvements over conventional models. However, when applied together, they produce small but consistent gains across most configurations. This observation suggests that while traditional imputers and classifiers are sufficient to validate the effectiveness of our proof-of-concept framework, the combined use of advanced architectures provides a promising direction for future enhancement, which we will discuss further in the concluding section.

TABLE V: Classification metrics (%) under VPFD augmentation scenarios.

Dataset	Metrics	MLP	LSTM	CNN1D	Transformer
VPFD	Acc	81.47	83.61	60.34	82.31
	FI _{bin}	80.10	82.90	59.20	81.72
	ROC-AUC	88.20	90.10	64.80	91.84
	PR-AUC	93.57	93.71	91.42	91.81
	FI _{macro}	86.50	89.18	90.53	82.30
	FI _{weighted}	86.50	89.18	90.53	82.29
	ECE	5.77	6.86	5.08	14.08
	Brier	9.63	8.26	7.53	15.31
	VPFD w/ EEG (MLP)	Acc	84.13	88.77	81.75
FI _{bin}		83.30	88.10	80.90	84.98
ROC-AUC		90.70	94.00	89.10	89.81
PR-AUC		82.51	83.32	84.16	81.63
FI _{macro}		76.59	77.14	76.22	78.19
FI _{weighted}		76.59	77.14	76.22	78.20
ECE		7.32	7.97	7.51	19.10
Brier		16.35	15.66	16.22	19.88
VPFD w/ EEG (TimeMixer)		Acc	82.90	81.00	73.50
	FI _{bin}	84.30	81.90	78.20	90.24
	ROC-AUC	86.60	83.90	79.80	96.17
	PR-AUC	82.51	83.32	84.16	95.47
	FI _{macro}	76.59	77.14	76.22	89.04
	FI _{weighted}	76.59	77.14	76.22	89.10
	ECE	7.32	7.97	7.51	9.32
	Brier	16.35	15.66	16.22	9.23
	VPFD w/ ECG (MLP)	Acc	84.14	86.99	81.55
FI _{bin}		83.40	86.20	80.60	82.93
ROC-AUC		90.60	93.20	88.80	88.16
PR-AUC		86.90	88.36	88.41	95.01
FI _{macro}		75.51	80.67	79.81	88.88
FI _{weighted}		75.70	80.78	79.92	88.92
ECE		7.78	7.76	6.74	9.76
Brier		14.97	13.66	13.88	10.15
VPFD w/ ECG (TimeMixer)		Acc	85.40	88.98	90.84
	FI _{bin}	86.73	90.05	91.06	92.54
	ROC-AUC	93.96	94.39	95.68	97.45
	PR-AUC	91.83	91.88	93.94	97.30
	FI _{macro}	85.25	88.85	90.84	92.56
	FI _{weighted}	85.25	88.86	90.84	92.56
	ECE	5.18	5.84	3.93	6.32
	Brier	9.80	8.65	7.01	6.78
	VPFD w/ EEG+ECG (MLP)	Acc	91.13	92.12	88.43
FI _{bin}		90.80	91.60	87.90	86.34
ROC-AUC		96.20	96.90	94.40	92.20
PR-AUC		89.47	86.97	86.39	91.83
FI _{macro}		81.39	76.67	79.58	84.90
FI _{weighted}		81.45	76.75	79.67	84.95
ECE		10.48	8.46	11.01	13.01
Brier		14.04	15.82	15.41	13.86
VPFD w/ EEG+ECG (TimeMixer)		Acc	87.80	92.61	92.29
	FI _{bin}	88.69	92.80	92.57	93.04
	ROC-AUC	95.39	96.88	95.08	97.88
	PR-AUC	93.66	96.30	88.44	97.71
	FI _{macro}	87.73	92.60	92.28	92.85
	FI _{weighted}	87.73	92.60	92.28	92.85
	ECE	5.39	5.64	4.11	6.38
	Brier	8.37	6.14	6.49	6.50

4) *Ablation of Batch Normalization and Jacobian Regularization*: The fourth experiments, summarized in Table VI, examines how different regularization strategies influence the quality of imputed modalities, ultimately, the resulting classification performance. The MLP classifier is used as the testbed in this experiment. An ablation study compares four settings—Batch Normalisation (BN) alone, Jacobian-norm regularization alone, both combined, and neither (serving as the baseline). BN smooths the feature distribution, while the Jacobian term sharpens the network’s sensitivity to the subtle variations required for reconstructing missing channels. When applied together, these mechanisms complement each other: BN provides a stable representation space and the Jacobian constraint enhances gradient information, allowing the model to recover absent modalities most faithfully and to achieve the best overall accuracy. This complementary effect is particularly evident in the configuration where both auxiliary sources are available, as the inclusion of multiple

reconstructed modalities (i.e., EEG+ECG) accentuates the performance gap between models with and without knowledge transfer. Although this study uses the MLP classifier for clarity of presentation, the underlying analysis indicates that the same synergy between distributional and gradient-based constraints is expected to generalize to other classifiers.

TABLE VI: Ablation study results (Accuracy %)

Method	VPFD w/ EEG	VPFD w/ ECG	VPFD w/ EEG+ECG
Baseline	81.78	81.20	83.68
BN	82.42	81.40	85.83
Jacobian	83.28	83.60	87.35
BN + Jacobian	84.14	84.13	91.13

5) *Sensitivity Tests*: Building on the previous results, where the combination of TimeMixer as the imputer and Transformer as the classifier achieved the better gains, we perform sensitivity tests under this configuration. Specifically, we evaluate the Transformer on VPFDEEG+ECG augmented using both FatigueSet and MEFAR via TimeMixer. The goal is to assess model robustness to input perturbations and hyperparameter variations (Fig.4).

For noise robustness, we inject zero-mean Gaussian noise with varying intensity σ into the standardized input features and fit a low-order regression of validation AUC against σ . The resulting curve remains nearly flat for small σ values and decreases smoothly as σ increases, indicating stability under mild perturbations and controlled degradation under stronger noise (Fig.4a).

For regularization, we vary the affine parameters (α, β) applied to standardized inputs as $x' = \alpha x + \beta$, and fit a smooth response surface of AUC over (α, β) . The surface exhibits a clear ridge at mid-range values, with performance declining only when α or β deviates substantially from their nominal values (e.g., $\alpha > 1$ or $|\beta| > 0.2$), indicating robustness to moderate calibration differences but sensitivity to extreme scaling or shifting. The results indicate that the model remains stable under small scaling and bias variations, which are typical in real-world deployments where sensor calibration and preprocessing may differ.

V. CONCLUSION

Fatigue detection is crucial in high stakes environments, where reduced alertness can have serious consequences. Despite advances in sensor technology, reliability and accessibility in real world environments remain major challenges, as many high-end sensors, such as EEG, are expensive, highly sensitive to environmental conditions, and require substantial operational setup outside controlled settings. To address this challenge, this paper proposes a proof-of-concept framework that enables knowledge transfer across differently instrumented sensor domains, aiming to enhance fatigue detection in real-world sensor-constrained scenarios. In particular, our approach transfers knowledge learned from high-fidelity laboratory sensors to field-deployable systems by using shared-channel overlap as a bridge, thereby maintaining detection accuracy when some modalities are unavailable. Our experiments provide empirical support for our claim and validate

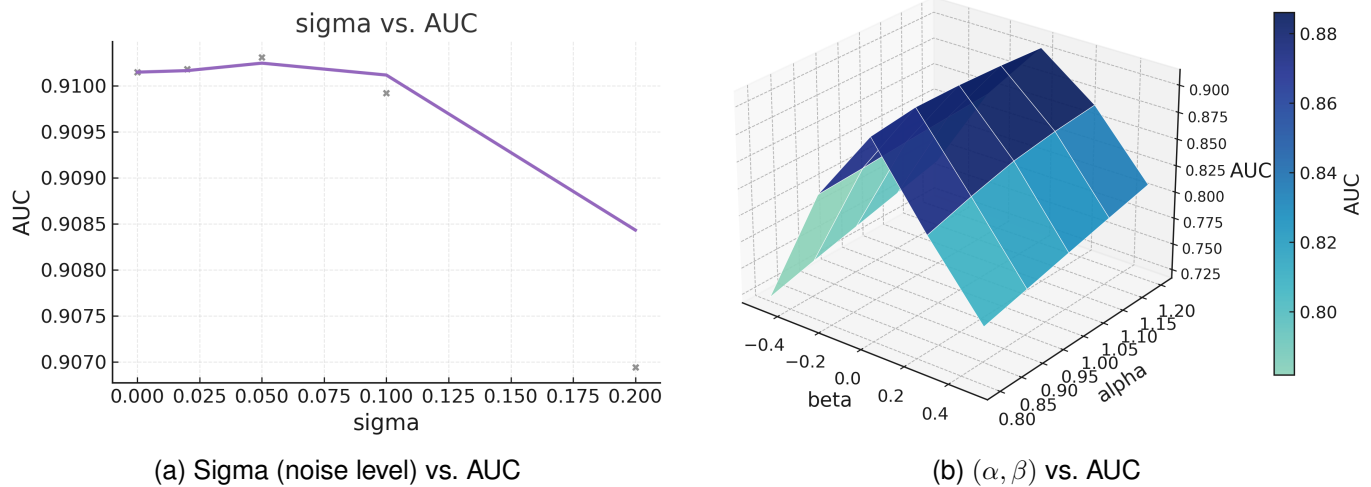


Fig. 4: Sensitivity analysis of the Transformer on VPF (EEG+ECG).

the framework's effectiveness and practicality, showing that transferred knowledge can substantially enhance detection when high-end sensors are unavailable.

The research can be extended in several directions. Although label heterogeneity is not present in our current case study, it remains an important factor for generalization in real-world applications. Differences in annotation subjectivity can introduce transfer bias and evaluation challenges. Thus approaches incorporating open-set recognition and label-shift calibration [66] are worth exploring to mitigate such bias. In addition, our experiments show that using TimerMixer and Transformer yields small but consistent gains over other traditional configurations. We will further this exploration in our future research, developing jointly optimized imputation and classifier architectures to better capture nonlinear dependencies and enhance fatigue-detection performance. Finally, as the framework continues to evolve, we plan to examine its real-time deployment aspects, focusing on computational efficiency, latency, and resource requirements to ensure suitability for field applications.

REFERENCES

- [1] R. Hooda, V. Joshi, M. Shah, A comprehensive review of approaches to detect fatigue using machine learning techniques, *Chronic Diseases and Translational Medicine* 8 (1) (2022) 26–35. doi:10.1016/j.cdtm.2021.07.002.
- [2] C. Zhu, L. Cui, Y. Tang, J. Wang, The evolution and future perspectives of artificial intelligence generated content (2025). arXiv:2412.01948. URL <https://arxiv.org/abs/2412.01948>
- [3] J. J. Bird, M. Pritchard, A. Fratini, A. Ekárt, D. R. Faria, Synthetic biological signals machine-generated by gpt-2 improve the classification of eeg and emg through data augmentation, *IEEE Robotics and Automation Letters* 6 (2) (2021) 3498–3504. doi:10.1109/LRA.2021.3056355.
- [4] A. G. Habashi, A. M. Azab, S. Eldawlatly, G. M. Aly, Motor imagery classification enhancement using generative adversarial networks for eeg spectrum image generation, in: 2023 IEEE 36th International Symposium on Computer-Based Medical Systems (CBMS), 2023, pp. 354–359. doi:10.1109/CBMS58004.2023.00243.
- [5] H. Zeng, X. Li, G. Borghini, Y. Zhao, P. Aricò, G. Di Flumeri, N. Sciarra, W. Zakaria, W. Kong, F. Babiloni, An eeg-based transfer learning method for cross-subject fatigue mental state prediction, *Sensors* 21 (7) (2021) 2369.
- [6] X. Zhang, M. Zeman, T. Tsiligkaridis, M. Zitnik, Graph-guided network for irregularly sampled multivariate time series, in: International Conference on Learning Representations, ICLR, 2022.
- [7] J. Hu, P. Wang, Noise robustness analysis of performance for eeg-based driver fatigue detection using different entropy feature sets, *Entropy* 19 (8) (2017). doi:10.3390/e19080385. URL <https://www.mdpi.com/1099-4300/19/8/385>
- [8] G. Borghini, G. Vecchiato, J. Toppi, L. Astolfi, A. Maglione, R. Isabella, C. Caltagirone, W. Kong, D. Wei, Z. Zhou, L. Polidori, S. Vitiello, F. Babiloni, Assessment of mental fatigue during car driving by using high resolution eeg activity and neurophysiologic indices, in: 2012 Annual International Conference of the IEEE Engineering in Medicine and Biology Society, 2012, pp. 6442–6445. doi:10.1109/EMBC.2012.6347469.
- [9] G. Sikander, S. Anwar, Driver fatigue detection systems: A review, *IEEE Transactions on Intelligent Transportation Systems* 20 (6) (2019) 2339–2352. doi:10.1109/TITS.2018.2868499.
- [10] A. Shahid, K. Wilkinson, S. Marcu, C. M. Shapiro, Stanford sleepiness scale (sss), in: A. Shahid, K. Wilkinson, S. Marcu, C. M. Shapiro (Eds.), *STOP, THAT and One Hundred Other Sleep Scales*, Springer New York, New York, NY, 2012, pp. 369–370.
- [11] E. Smets, B. Garssen, B. Bonke, J. De Haes, The multidimensional fatigue inventory (mfi) psychometric qualities of an instrument to assess fatigue, *Journal of psychosomatic research* 39 (3) (1995) 315–25.
- [12] F. B. Ortega, J. R. Ruiz, V. España-Romero, G. Vicente-Rodriguez, D. Martínez-Gómez, Y. Manios, L. Béghin, D. Molnar, K. Widhalm, L. A. Moreno, M. Sjöström, M. J. Castillo, The international fitness scale (ifis): usefulness of self-reported fitness in youth, *International Journal of Epidemiology* 40 (3) (2011) 701–711. doi:10.1093/ije/dyr039.
- [13] V. J. Gawron, Overview of self-reported measures of fatigue, *The International Journal of Aviation Psychology* 26 (3-4) (2016) 120–131.
- [14] N. Brown, S. Bichler, M. Fiedler, W. Alt, Fatigue detection in strength training using three-dimensional accelerometry and principal component analysis, *Sports biomechanics* 15 (2) (2016) 139–150.
- [15] B. T. Jap, S. Lal, P. Fischer, E. Bekiaris, Using eeg spectral components to assess algorithms for detecting fatigue, *Expert Systems with Applications* 36 (2) (2009) 2352–2359.
- [16] S. Kar, M. Bhagat, A. Routray, Eeg signal analysis for the assessment and quantification of driver's fatigue, *Transportation research part F: traffic psychology and behaviour* 13 (5) (2010) 297–306.
- [17] S. Fu, Z. Yang, Y. Ma, Z. Li, L. Xu, H. Zhou, Advancements in the intelligent detection of driver fatigue and distraction: A comprehensive review, *Applied Sciences* 14 (7) (2024). doi:10.3390/app14073016.
- [18] R. Olaganathan, T. Holt, J. Luedtke, B. Bowen, Fatigue and its management in the aviation industry, with special reference to pilots, *Journal of*

- Aviation Technology and Engineering 10 (2021) 45. doi:10.7771/2159-6670.1208.
- [19] G. Li, W. Yan, S. Li, X. Qu, W. Chu, D. Cao, A temporal-spatial deep learning approach for driver distraction detection based on eeg signals, *IEEE Transactions on Automation Science and Engineering* 19 (4) (2022) 2665–2677. doi:10.1109/TASE.2021.3088897.
- [20] P. Zhao, C. Lian, B. Xu, Z. Zeng, Multiscale global prompt transformer for eeg-based driver fatigue recognition, *IEEE Transactions on Automation Science and Engineering* 22 (2025) 2700–2711. doi:10.1109/TASE.2024.3382892.
- [21] Q. Wu, C. Xi, L. Ding, C. Wei, H. Ren, R. Law, H. Dong, X. L. Li, Classification of emg signals by bfa-optimized gsvcm for diagnosis of fatigue status, *IEEE Transactions on Automation Science and Engineering* 14 (2) (2017) 915–930. doi:10.1109/TASE.2016.2564419.
- [22] S. Chand, A. J. McDaid, Y. Lu, Isometric-based approach for detecting localized muscular fatigue during complex dynamic manufacturing operations, in: 2021 IEEE 17th International Conference on Automation Science and Engineering (CASE), 2021, pp. 1940–1945. doi:10.1109/CASE49439.2021.9551478.
- [23] H. Al-Libawy, A. Al-Ataby, W. Al-Nuaimy, M. A. Al-Tae, Hrv-based operator fatigue analysis and classification using wearable sensors, in: 2016 13th International Multi-Conference on Systems, Signals & Devices (SSD), 2016, pp. 268–273. doi:10.1109/SSD.2016.7473750.
- [24] R. Markiewicz, A. Markiewicz-Gospodarek, B. Dobrowolska, Galvanic skin response features in psychiatry and mental disorders: A narrative review, *International Journal of Environmental Research and Public Health* 19 (20) (2022) 13428. doi:10.3390/ijerph192013428.
- [25] Y. Jiao, C. Zhang, X. Chen, L. Fu, C. Jiang, C. Wen, Driver fatigue detection using measures of heart rate variability and electrodermal activity, *IEEE Transactions on Intelligent Transportation Systems* 25 (6) (2024) 5510–5524. doi:10.1109/ITITS.2023.3333252.
- [26] K. Mohanavelu, R. Lamshe, S. Poonguzhali, K. Adalarasu, M. Jagannath, Assessment of human fatigue during physical performance using physiological signals: A review, *Biomedical and Pharmacology Journal* 10 (4) (2017) 1887–1896.
- [27] L. J. Trejo, K. Kubitz, R. Rosipal, R. L. Kochavi, L. D. Montgomery, Eeg-based estimation and classification of mental fatigue, *Psychology* 6 (5) (2015) 572–589.
- [28] S.-Y. Cheng, H.-T. Hsu, Mental fatigue measurement using eeg, in: *Risk management trends*, IntechOpen, 2011.
- [29] T. G. Monteiro, C. Skourup, H. Zhang, Using eeg for mental fatigue assessment: A comprehensive look into the current state of the art, *IEEE Transactions on Human-Machine Systems* 49 (6) (2019) 599–610.
- [30] J. LaRocco, M. D. Le, D.-G. Paeng, A systemic review of available low-cost eeg headsets used for drowsiness detection, *Frontiers in neuroinformatics* 14 (2020) 553352.
- [31] R. Shashidhar, S. Hariprasad, B. SHRUTHI, R. S. KAVITA, Real-time fatigue detection using a low cost wireless eeg device, *i-Manager's Journal on Embedded Systems* 8 (2) (2020) 8–13.
- [32] F. Liu, D. Chen, J. Zhou, F. Xu, A review of driver fatigue detection and its advances on the use of rgb-d camera and deep learning, *Engineering Applications of Artificial Intelligence* 116 (2022) 105399. doi:https://doi.org/10.1016/j.engappai.2022.105399.
- [33] Y. Yi, Z. Zhou, W. Zhang, M. Zhou, Y. Yuan, C. Li, Fatigue detection algorithm based on eye multifeature fusion, *IEEE Sensors Journal* 23 (7) (2023) 7949–7955. doi:10.1109/JSEN.2023.3247582.
- [34] W. Deng, R. Wu, Real-time driver-drowsiness detection system using facial features, *IEEE Access* 7 (2019) 118727–118738. doi:10.1109/ACCESS.2019.2936663.
- [35] H. Zheng, S. Chand, A. Keshvarparast, D. Battini, Y. Lu, Video-based fatigue estimation for human-robot task allocation optimisation, in: 2023 IEEE 19th International Conference on Automation Science and Engineering (CASE), 2023, pp. 1–6. doi:10.1109/CASE56687.2023.10260460.
- [36] X. Li, W. Xu, B. Yao, Z. Ji, X. Liu, Dynamic task reallocation in human-robot collaborative workshop based on online biotic fatigue detection, in: 2022 IEEE 18th International Conference on Automation Science and Engineering (CASE), 2022, pp. 116–122. doi:10.1109/CASE49997.2022.9926591.
- [37] S. Yanqing, D. Pengfei, Z. Yangjing, C. Shitao, Z. Nanning, Privacy protection of sensitive bioinformation based on event cameras, *Strategic Study of CAE* 26 (1) (2024). doi:10.15302/J-SSCAE-2024.01.017.
- [38] K. Krejtz, A. T. Duchowski, A. Niedzielska, C. Biele, I. Krejtz, Eye tracking cognitive load using pupil diameter and microsaccades with fixed gaze, *PLoS one* 13 (9) (2018) e0203629.
- [39] F. N. Biondi, F. Graf, J. Cort, Testing pupil size as a possible alternative metric of physical fatigue in automotive manufacturing tasks, *Proceedings of the Human Factors and Ergonomics Society Annual Meeting* 67 (1) (2023) 824–828. doi:10.1177/21695067231192895.
- [40] N. Y. Yair Morad, Hadas Lemberg, Y. Dagan, Pupillography as an objective indicator of fatigue, *Current Eye Research* 21 (1) (2000) 535–542. doi:10.1076/0271-3683(200007)2111-ZFT535.
- [41] L. Cui, Y. Wu, Y. Tang, Generalizable gaze synthesis for practical fatigue detection systems, in: 2024 International Conference on Cyber-Physical Social Intelligence (ICCSI), 2024, pp. 1–6. doi:10.1109/ICCSI62669.2024.10799435.
- [42] N. Neifar, A. Mdhaffar, A. Ben-Hamadou, M. Jmaiel, Deep generative models for physiological signals: A systematic literature review, *Artificial Intelligence in Medicine* 165 (2025) 103127. doi:https://doi.org/10.1016/j.artmed.2025.103127. URL <https://www.sciencedirect.com/science/article/pii/S0933365725000624>
- [43] O. Kulkarni, R. Chandra, Bayes-catsi: A variational bayesian deep learning framework for medical time series data imputation (2024). arXiv:2410.01847. URL <https://arxiv.org/abs/2410.01847>
- [44] F. M. Zahid, C. Heumann, Multiple imputation with sequential penalized regression, *Statistical Methods in Medical Research* 28 (5) (2019) 1311–1327, epub 2018 Feb 16. doi:10.1177/0962280218755574. URL <https://doi.org/10.1177/0962280218755574>
- [45] Y. Deng, C. Chang, M. S. Ido, Q. Long, Multiple imputation for general missing data patterns in the presence of high-dimensional data, *Scientific Reports* 6 (1) (2016) 21689. doi:10.1038/srep21689. URL <https://doi.org/10.1038/srep21689>
- [46] Z. Che, S. Purushotham, K. Cho, D. Sontag, Y. Liu, Recurrent neural networks for multivariate time series with missing values, in: *Proceedings of the 2016 ACM SIGKDD International Conference on Knowledge Discovery and Data Mining*, ACM, 2016, pp. 749–758.
- [47] A. Verma, A. Kumar, An accurate missing data prediction method using lstm based deep learning for health care, *Procedia Computer Science* 167 (2019) 2414–2423.
- [48] W. Cao, D. Wang, J. Li, H. Zhou, S. Li, Y. He, Y. Liu, H. Zha, Brits: Bidirectional recurrent imputation for time series, arXiv preprint arXiv:1805.10572 (2018).
- [49] Y. Eum, E.-H. Yoo, Imputation of missing time-activity data with long-term gaps: A multi-scale residual cnn-lstm network model, *Computers, Environment and Urban Systems* 95 (2022) 101823. doi:10.1016/j.compenvurbsys.2022.101823.
- [50] S. Behera, R. Misra, A. Sillitti, Gan-based multi-task learning approach for prognostics and health management of iiot, *IEEE Transactions on Automation Science and Engineering* 21 (3) (2024) 2742–2762. doi:10.1109/TASE.2023.3267860.
- [51] W. Li, C. Gu, J. Chen, C. Ma, X. Zhang, B. Chen, S. Wan, Dls-gan: Generative adversarial nets for defect location sensitive data augmentation, *IEEE Transactions on Automation Science and Engineering* 21 (4) (2024) 5173–5189. doi:10.1109/TASE.2023.3309629.
- [52] A. F. Nia, V. Tang, G. M. Talou, M. Billinghurst, Synthesizing affective neurophysiological signals using generative models: A review paper, *Journal of Neuroscience Methods* 406 (2024) 110129. doi:https://doi.org/10.1016/j.jneumeth.2024.110129. URL <https://www.sciencedirect.com/science/article/pii/S0165027024000748>
- [53] M. Kalanadhabhatta, C. Min, A. Montanari, F. Kawsar, Fatigueset: A multi-modal dataset for modeling mental fatigue and fatigability, in: H. Lewy, R. Barkan (Eds.), *Pervasive Computing Technologies for Healthcare*, Springer International Publishing, Cham, 2022, pp. 204–217.
- [54] S. Derdiyok, F. P. Akbulut, C. Catal, Neurophysiological and biosignal data for investigating occupational mental fatigue: Mefar dataset, *Data in Brief* 52 (2024) 109896. doi:https://doi.org/10.1016/j.dib.2023.109896.
- [55] M. Papakostas, A. Rajavenkatanarayanan, F. Makedon, Cogbeacon: A multi-modal dataset and data-collection platform for modeling cognitive fatigue, *Technologies* 7 (2) (2019). doi:10.3390/technologies7020046.
- [56] V. Markova, T. Ganchev, K. Kalinkov, Clas: A database for cognitive load, affect and stress recognition, in: 2019 International Conference on Biomedical Innovations and Applications (BIA), 2019, pp. 1–4. doi:10.1109/BIA48344.2019.8967457.
- [57] M. Gabbi, L. Cornia, V. Villani, L. Sabattini, Understanding fatigue through biosignals: A comprehensive dataset, 2024 19th ACM/IEEE International Conference on Human-Robot Interaction (HRI) (2024) 901–905.

- [58] S. Kovalenko, A. Mamonov, V. Kuznetsov, A. Bulygin, I. Shoshina, I. Brak, A. Kashevnik, Operatoroyevp: Operator dataset for fatigue detection based on eye movements, heart rate data, and video information, *Sensors* 23 (13) (2023). doi:10.3390/s23136197.
- [59] P. Schmidt, A. Reiss, R. Duerichen, C. Marberger, K. Van Laerhoven, Introducing wesad, a multimodal dataset for wearable stress and affect detection, in: *Proceedings of the 20th ACM International Conference on Multimodal Interaction, ICMI '18*, Association for Computing Machinery, New York, NY, USA, 2018, p. 400–408. doi:10.1145/3242969.3242985.
- [60] Y. Bu, S. Zou, V. V. Veeravalli, Tightening Mutual Information Based Bounds on Generalization Error (2019) 12.
- [61] Y. Mansour, M. Mohri, A. Rostamizadeh, Domain adaptation: Learning bounds and algorithms, arXiv preprint arXiv:0902.3430 (2009).
- [62] S. Ioffe, C. Szegedy, Batch normalization: Accelerating deep network training by reducing internal covariate shift (2015). arXiv:1502.03167. URL <https://arxiv.org/abs/1502.03167>
- [63] W. Li, S. Chen, Partial domain adaptation without domain alignment, *IEEE Transactions on Pattern Analysis and Machine Intelligence* 45 (7) (2023) 8787–8797. doi:10.1109/tpami.2022.3228937. URL <http://dx.doi.org/10.1109/TPAMI.2022.3228937>
- [64] M. Kalanadhabhatta, C. Min, A. Montanari, F. Kawsar, Fatigueset: A multi-modal dataset for modeling mental fatigue and fatigability, in: *International Conference on Pervasive Computing Technologies for Healthcare*, Springer, 2021, pp. 204–217.
- [65] S. Wang, H. Wu, X. Shi, T. Hu, H. Luo, L. Ma, J. Y. Zhang, J. Zhou, Timemixer: Decomposable multiscale mixing for time series forecasting (2025). arXiv:2405.14616. URL <https://arxiv.org/abs/2405.14616>
- [66] P. Yang, H. Yang, H. Fu, D. Zhou, J. Ye, T. Lappas, J. He, Jointly modeling label and feature heterogeneity in medical informatics, *ACM Trans. Knowl. Discov. Data* 10 (4) (May 2016). doi:10.1145/2768831. URL <https://doi.org/10.1145/2768831>



Ying Tang (Senior Member, IEEE) received the B.S. and M.S. degrees from the Northeastern University, P. R. China, in 1996 and 1998, respectively, and Ph. D degree from New Jersey Institute of Technology in 2001. She is currently Full Professor and the Undergraduate Program Chair of Electrical and Computer Engineering at Rowan University, Glassboro, New Jersey. Her current research interest lies in the area of cyber-physical social systems, extended reality, adaptive and personalized systems, modeling and adaptive control for computer-integrated systems, and sustainable production automation. Her work has been continuously supported by NSF, EPA, US Army, FAA, DOT, private foundations, and industry. She has three USA patents, and over 250 peer-reviewed publications, including 88 journal articles, 2 edited books, and 6 book/ encyclopedia chapters. Dr. Tang is presently Associate Editor of *IEEE Transactions on Systems, Man, and Cybernetics: Systems*, *IEEE Transactions on Intelligent Vehicles*, *IEEE Transactions on Computational Social Systems*, and Springer's *Discover Artificial Intelligence*. She is the Founding Chair of Technical Committee on Intelligent Solutions to Human-aware Sustainability for IEEE Systems, Man, & Cybernetic, and the Founding Chair of Technical Committee on Sustainable Production Automation for IEEE Robotic and Automation.



educational games to enhance student comprehension in science, technology, and engineering fields.

LuoBin Cui (Member, IEEE) received the B.S. degree from Jiangsu University of Technology, P.R. China, in 2020, and the M.S. degree from Monmouth University, USA, in 2022. He is currently pursuing the Ph.D. degree in Electrical and Computer Engineering at Rowan University, USA. His research interests include machine learning, and artificial intelligence, with a particular focus on Graph Neural Networks and their applications. He has also conducted research on fatigue detection using physiological data and explored the development of



Laboratory of Pattern Analysis and Machine Intelligence (PAMI), Nanjing, and China Science IntelliCloud Technology, Hefei, China.

His research interests include pattern recognition and machine learning.

Weikai Li received his B.S. degree in Information and Computing Science (2015) and M.S. degree in Computer Science and Technology (2018) from Chongqing Jiaotong University, Chongqing, China. He obtained his Ph.D. degree in Computer Science and Technology from the College of Computer Science and Technology, Nanjing University of Aeronautics and Astronautics, Nanjing, China, in 2022.

He is currently a Lecturer at the School of Mathematics and Statistics, Chongqing Jiaotong University. He is also a Researcher with the MIIT Key



Yanlai Wu received the B.S. degree in Artificial Intelligence from the School of Information Science and Engineering, Chongqing Jiaotong University, Chongqing, China. He is currently pursuing the M.S. degree in Electrical and Computer Engineering with the School of Engineering, Rowan University, USA.

His current research interests include pattern recognition, computer vision, and natural language processing.

APPENDIX

Lemma 1. [60] Suppose the loss function $\mathcal{L}(f(x), y)$ is R -sub-Gaussian under $x \sim \mathbb{P}$ for all $y \in \mathcal{Y}$, then, we have:

$$\mathcal{E}_{\mathbb{P}}(f) \leq \mathcal{E}_{\hat{\mathbb{P}}}(f) + \sqrt{\frac{2R^2}{n} I(x, y)} \quad (6)$$

where n is the number of the training samples and $I(x, y)$ is the mutual information between x and y .

Theorem 1. Assume that x, a are independent of each other, $x \sim \mathbb{P}, a \sim \mathbb{Q}_a$, while both being conditionally dependent on variable of y , Let the composite observation be defined as $x^+ = [x, a], x^+ \sim \mathbb{P}_+$, with the incorporating the variable a , the $\mathcal{E}_{\mathbb{P}_+}$ have a tighten upper bound than $\mathcal{E}_{\mathbb{P}}$, the gap G is:

$$G = \Delta + \sqrt{\frac{2R^2}{n}} \left(\sqrt{I(x^+, y)} - \sqrt{I(x, y)} \right) < 0 \quad (7)$$

where $\Delta = \mathcal{E}_{\mathbb{P}_+} - \mathcal{E}_{\hat{\mathbb{P}}}$. The proof is given in the Appendix. Following **Theorem 1**, it is evident that incorporating label-related features/sensors (i.e., a) can effectively reduce the generalization error bound, thereby enhancing the generalization performance.

Proof: For $\mathcal{E}_{\hat{\mathbb{P}}}(f)$ and $\mathcal{E}_{\hat{\mathbb{P}}_+}(f)$, we have:

$$\begin{aligned} \mathcal{E}_{\hat{\mathbb{P}}}(f) &= \mathcal{L}(f(x), y) \\ \mathcal{E}_{\hat{\mathbb{P}}_+}(f) &= \mathcal{L}(f([x, a]), y) \end{aligned} \quad (8)$$

note that the x, a are independent of each other, x, a are depend of y , thus, we can easily have:

$$\Delta = \mathcal{E}_{\hat{\mathbb{P}}_+} - \mathcal{E}_{\hat{\mathbb{P}}} \leq 0 \quad (9)$$

For $\sqrt{\frac{2R^2}{n}} \left(\sqrt{I(x^+, y)} - \sqrt{I(x, y)} \right)$, since $\sqrt{\frac{2R^2}{n}} > 0$, $I(x^+, y) \geq 0$ and $I(x, y) \geq 0$. Thus, The positivity or negativity of the expression can be determined by $I(x^+, y) - I(x, y)$. Then we have:

$$\begin{aligned} I(x^+, y) - I(x, y) &= H(Y) - H(Y|x^+) - (H(Y) - H(Y|x)) \\ &= H(Y|x) - H(Y|x^+) \end{aligned} \quad (10)$$

where $H(\cdot)$ is the entropy, since $x^+ = [x, a]$, x, a are independent of each other, x, a are depend of y , $H(Y|x^+) - H(Y|x) < 0$, then we have:

$$I(x^+, y) - I(x, y) = H(Y|x) - H(Y|x^+) < 0 \quad (11)$$

According to Eq. 11, we easily have:

$$\sqrt{\frac{2R^2}{n}} \left(\sqrt{I(x^+, y)} - \sqrt{I(x, y)} \right) < 0 \quad (12)$$

Combining Eqs 9 and 12, we have:

$$G = \Delta + \sqrt{\frac{2R^2}{n}} \left(\sqrt{I(x^+, y)} - \sqrt{I(x, y)} \right) < 0 \quad (13)$$

Thus, with the incorporates of the new sensors, the $\mathcal{E}_{\mathbb{P}}$ have a tighten upper bound.

Q.E.D

Theorem 2. Given a random variable \hat{a} generated from a distribution $\mathbb{Q}_{\hat{a}}$, and $\hat{x}^+ = [x, \hat{a}] \sim \mathbb{Q}$, then we have:

$$\mathcal{E}_{\mathbb{P}_+}(f) \leq \mathcal{E}_{\hat{\mathbb{Q}}}(f) + \epsilon_{ideal} + d_{\mathcal{H}\Delta\mathcal{H}}(\mathbb{Q}_a, \mathbb{Q}_{\hat{a}}) + \sqrt{\frac{2R^2}{n} I(x, y)} \quad (14)$$

where $\mathcal{E}_{\hat{\mathbb{Q}}}(f)$ is the empirical generalization error over distribution \mathbb{Q} , $d_{\mathcal{H}\Delta\mathcal{H}}(\mathbb{Q}_a, \mathbb{Q}_{\hat{a}})$ is the $\mathcal{H}\Delta\mathcal{H}$ distance between \mathbb{Q}_a and $\mathbb{Q}_{\hat{a}}$.

Before we proof the **Theorem 2**, we need the following Definition:

Definition 1 (Disparity). Given two classifier f and f' , the disparity between two classifier f and f' over the distribution \mathbb{P} is as follows:

$$\mathcal{E}_{\mathbb{P}}(f, f') = \mathbb{E}_{x \sim \mathbb{P}} [f(x) \neq f'(x)] \quad (15)$$

Definition 2 (Ideal Classifier). Given two Distribution \mathbb{P} and \mathbb{Q} the ideal classifier f^* have the minimum risk over two distributions as follows:

$$f^* = \arg \min_f (\mathcal{E}_{\mathbb{P}}(f) + \mathcal{E}_{\mathbb{P}}(f)) \quad (16)$$

Definition 3 ($\mathcal{H}\Delta\mathcal{H}$ distance). Given two Distribution \mathbb{P} and \mathbb{Q} , the $\mathcal{H}\Delta\mathcal{H}$ distance between \mathbb{P} and \mathbb{Q} is defined as follows:

$$d_{\mathcal{H}\Delta\mathcal{H}}(\mathbb{P}, \mathbb{Q}) = \sup_{f, f' \in \mathcal{H}} |\mathcal{E}_{\mathbb{P}}(f, f') - \mathcal{E}_{\mathbb{Q}}(f, f')| \quad (17)$$

where \mathcal{H} is the Hypothesis space.

Assumption: the ideal classifier has a small risk.

$$\epsilon_{ideal} = (\mathcal{E}_{\mathbb{P}}(f^*) + \mathcal{E}_{\mathbb{P}}(f^*)) \quad (18)$$

Proof:

By using the triangle inequalities, we have

$$\begin{aligned} \mathcal{E}_{\mathbb{P}_+}(f) &\leq \mathcal{E}_{\mathbb{P}_+}(f^*) + \mathcal{E}_{\mathbb{P}_+}(f, f^*) \\ &\leq \mathcal{E}_{\mathbb{P}_+}(f^*) + \mathcal{E}_{\mathbb{Q}}(f, f^*) + \mathcal{E}_{\mathbb{P}_+}(f, f^*) - \mathcal{E}_{\mathbb{Q}}(f, f^*) \\ &\leq \mathcal{E}_{\mathbb{P}_+}(f^*) + \mathcal{E}_{\mathbb{Q}}(f, f^*) + |\mathcal{E}_{\mathbb{P}_+}(f, f^*) - \mathcal{E}_{\mathbb{Q}}(f, f^*)| \\ &\leq \mathcal{E}_{\mathbb{Q}}(f) + \mathcal{E}_{\mathbb{Q}}(f^*) + \mathcal{E}_{\mathbb{P}_+}(f^*) + |\mathcal{E}_{\mathbb{P}_+}(f, f^*) - \mathcal{E}_{\mathbb{Q}}(f, f^*)| \end{aligned} \quad (19)$$

According to definition of ideal classifier and $\mathcal{H}\Delta\mathcal{H}$ distance we have:

$$\begin{aligned} \mathcal{E}_{\mathbb{P}_+}(f) &\leq \mathcal{E}_{\mathbb{Q}}(f) + \mathcal{E}_{\mathbb{Q}}(f^*) + \mathcal{E}_{\mathbb{P}_+}(f^*) + |\mathcal{E}_{\mathbb{P}_+}(f, f^*) - \mathcal{E}_{\mathbb{Q}}(f, f^*)| \\ &= \mathcal{E}_{\mathbb{Q}}(f) + \epsilon_{ideal} + |\mathcal{E}_{\mathbb{P}_+}(f, f^*) - \mathcal{E}_{\mathbb{Q}}(f, f^*)| \\ &\leq \mathcal{E}_{\mathbb{Q}}(f) + \epsilon_{ideal} + d_{\mathcal{H}\Delta\mathcal{H}}(\mathbb{P}_+, \mathbb{Q}) \end{aligned} \quad (20)$$

According to Lemma 1, we have:

$$\mathcal{E}_{\mathbb{P}_+}(f) \leq \mathcal{E}_{\hat{\mathbb{P}}_+}(f) + \sqrt{\frac{2R^2}{n} I(x, y)} \quad (21)$$

Note that $\hat{x}^+ = [x, \hat{a}]$ and $x^+ = [x, a]$, we further have:

$$\begin{aligned} d_{\mathcal{H}\Delta\mathcal{H}}(\mathbb{P}_+, \mathbb{Q}) &\leq d_{\mathcal{H}\Delta\mathcal{H}}(\mathbb{P}, \mathbb{P}) + d_{\mathcal{H}\Delta\mathcal{H}}(\mathbb{Q}_a, \mathbb{Q}_{\hat{a}}) \\ &\leq d_{\mathcal{H}\Delta\mathcal{H}}(\mathbb{Q}_a, \mathbb{Q}_{\hat{a}}) \end{aligned} \quad (22)$$

By plugging Lemma 1 and Eq.22 into Eq. 20, we have:

$$\mathcal{E}_{\mathbb{P}}(f) \leq \mathcal{E}_{\hat{\mathbb{Q}}}(f) + \epsilon_{ideal} + d_{\mathcal{H}\Delta\mathcal{H}}(\mathbb{Q}_a, \mathbb{Q}_{\hat{a}}) + \sqrt{\frac{2R^2}{n}I(x, y)} \quad (23)$$

Q.E.D

Lemma 2. [61] *Let S and T be the source and target domains over $\mathcal{X} \times \mathcal{Y}$, respectively. Let \mathcal{H} be a hypothesis class, and let $\ell : \mathcal{Y} \times \mathcal{Y} \rightarrow \mathbb{R}_+$ be a loss function that is symmetric, obeys the triangle inequality, and is bounded, $\forall (y, y') \in \mathcal{Y}^2$, $\ell(y, y') \leq M$ for some $M > 0$. Then, for $h_S^* = \arg \min_{h \in \mathcal{H}} R_S^\ell(h)$ and $h_T^* = \arg \min_{h \in \mathcal{H}} R_T^\ell(h)$ denoting the ideal hypotheses for the source and target domains, we have*

$$\forall h \in \mathcal{H}, R_T^\ell(h) \leq R_S^\ell(h, h_S^*) + d_{\mathcal{H}\Delta\mathcal{H}}(\mathbb{P}_S, \mathbb{P}_T) + \epsilon, \quad (24)$$

where $R_S^\ell(h, h_S^*) = \mathbb{E}_{x \sim S_X} \ell(h(x), h_S^*(x))$ and $\epsilon = R_T^\ell(h_T^*) + R_S^\ell(h_T^*, h_S^*)$.

Theorem 3. *Let \mathcal{H} be a hypothesis class. $R_S^\ell(g)$ and $R_T^\ell(g)$ denote the expected loss of loss function ℓ for the source and target domains. for $g_s^* = \arg \min_{g \in \mathcal{H}} R_S^\ell(g)$ and $g_T^* = \arg \min_{g \in \mathcal{H}} R_T^\ell(g)$ denoting the ideal hypotheses for the source and target domains, we have*

$$R_T^\ell(g_s) \leq R_S^\ell(g_s, g_s^*) + d_{\mathcal{H}\Delta\mathcal{H}}(\mathbb{P}_T^\square, \mathbb{P}_S^\square) + \epsilon, \quad (25)$$

where $R_S^\ell(g_s, g_s^*) = \mathbb{E}_{x \sim \mathbb{P}_s} \ell(g_s(x), g_s^*(x))$ and $\epsilon = R_T^\ell(g_T^*) + R_S^\ell(g_T^*, g_s^*)$.

Proof: The proof of Theorem 3 can be obtained by substituting the variables in Lemma 2, so the proof is omitted.